Mutations in a TGFß ligand, *TGFB3*, cause syndromic aortic aneurysms and dissections

Aida M. Bertoli-Avella*, Elisabeth Gillis*, Hiroko Morisaki*, Judith M.A. Verhagen, Bianca M. de Graaf, Gerarda van de Beek, Elena Gallo, Boudewijn P.T. Kruithof, Hanka Venselaar, Loretha Myers, Steven Laga, Alex J. Doyle, Gretchen Oswald, Gert W.A. van Cappellen, Itaru Yamanaka, Robert M. van der Helm, Berna Beverloo, Annelies de Klein, Luba Pardo, Martin Lammens, Christina Evers, Koen Devriendt, Michiel Dumoulein, Janneke Timmermans, Hennie T. Brüggenwirth, Frans W. Verheijen, Inez Rodrigus, Gareth Baynam, Marlies Kempers, Johan Saenen, Emeline M. Van Craenenbroeck, Kenji Minatoya, Ritsu Matsukawa, Takuro Tsukube, Noriaki Kubo, Robert M.W. Hofstra, Marie-José Goumans, Jos A. Bekkers, Jolien W. Roos-Hesselink, Ingrid M.B.H. van de Laar, Harry C. Dietz, Lut van Laer, Takayuki Morisaki*, Marja W. Wessels*, Bart L. Loeys*

**These authors contributed equally*

Journal of the American College of Cardiology 2015;65(13):1324-1336

Abstract

Background

Aneurysms affecting the aorta are a common condition associated with high mortality due to aortic dissection or rupture. Investigations of the pathogenic mechanisms involved in syndromic types of thoracic aortic aneurysms such as Marfan and Loeys-Dietz syndromes, have revealed an important contribution of disturbed TGFβ signaling.

Objective

To discover a novel gene causing syndromic aortic aneurysms in order to unravel the underlying pathogenesis.

Methods

We combined genome wide linkage analysis, exome sequencing and candidate gene Sanger sequencing in a total of 470 index cases with thoracic aortic aneurysms. Extensive cardiologic examination, including physical examination, electrocardiography and transthoracic echocardiography was performed. In adults, imaging of the entire aorta using computed tomography or magnetic resonance imaging was done.

Results

Here we report on 43 patients from 11 families with syndromic presentations of aortic aneurysms caused by *TGFB3* mutations. We demonstrate that *TGFB3* mutations are associated with significant cardiovascular involvement, including thoracic/abdominal aortic aneurysm and dissection and mitral valve disease. Other systemic features overlap clinically with Loeys-Dietz, Shprintzen-Goldberg and Marfan syndrome, including cleft palate, bifid uvula, skeletal overgrowth, cervical spine instability and club foot deformity. In line with previous observations in aortic wall tissues of patients with mutations in effectors of TGFβ signaling (*TGFBR1/2, SMAD3* and *TGFB2*), we confirm a paradoxical upregulation of both canonical and non-canonical TGFβ signaling in association with upregulation of expression of TGFβ ligands.

Conclusions

Our findings emphasize the broad clinical variability associated with *TGFB3* mutations and highlight the importance of early recognition of the disease due to high cardiovascular risk.

Introduction

The TGFβ pathway plays an important role in many medically relevant processes including immunologic maturity, inflammation, cancer and fibrosis as well as skeletal, vascular and hematopoietic homeostasis [1]. With the discovery of dysregulated TGFβ signaling in *Fbn1* knockout mice, the TGFβ pathway was revealed as a key player in the pathogenesis of thoracic aortic aneurysm development in Marfan syndrome (MFS; [MIM 154700]) [2, 3]. MFS is a multisystemic disease characterized by cardiovascular, ocular and skeletal features caused by mutations in the *FBN1* gene [4]. More recently, we and others identified pathogenic mutations in the genes encoding the TGFβ receptor subunits TGFBR1 and TGFBR2 [5, 6], the signaling transducer SMAD3 [7], the ligand TGFB2 [8, 9] and the inhibitor SKI [10], occurring predominantly in patients with syndromic presentations of thoracic aortic aneurysms and dissections (TAAD), designated Loeys-Dietz syndrome (LDS1 [MIM 609192] [11]; LDS2 [MIM 610168] [11]; LDS3 [MIM 613795] a.k.a. aneurysms-osteoarthritis syndrome [7, 12, 13], LDS4 [MIM 614816]) [8] and Shprintzen-Goldberg syndrome (SGS [MIM 82212]) [13, 14]. The finding of human mutations in a ligand, receptors, a signaling transducer and an inhibitor of the TGFβ pathway confirm the essential role of TGFβ signaling in aortic aneurysm development.

Recently, *de novo* mutations in the gene encoding the TGFB3 ligand (*TGFB3*) were reported in two girls exhibiting a syndrome affecting body growth (either short or tall stature) accompanied by skeletal features reminiscent of MFS or LDS, but without significant vascular involvement [15-17]. Here we report that *TGFB3* mutations cause a syndromic form of aortic aneurysms and dissections, which is characterized by cardiovascular, craniofacial, cutaneous and skeletal anomalies that significantly overlap with other TGFβ vasculopathies, particularly those within the LDS clinical spectrum.

Methods

Patients

All patients or relatives provided written informed consent for participation in this study and, if applicable, publication of photographs. Family 1 was investigated by the department of Clinical Genetics (Erasmus University Medical Center, Rotterdam, the Netherlands) and Center for Medical Genetics (Antwerp University Hospital/University of Antwerp, Belgium) after previous surgical interventions. Family members were examined by clinical geneticists (M.W.W., B.L.L.) with special attention to skeletal, joint, skin and craniofacial features. Medical records from deceased patients were obtained for review. Extensive cardiologic examination, including physical examination, electrocardiography and transthoracic echocardiography was performed. In adults, imaging of the entire aorta using computed tomography or magnetic

resonance imaging was performed. Measurements of the aortic diameter were obtained at the level of the aortic annulus, sinuses of Valsalva, sinotubular junction, proximal ascending aorta, aortic arch, descending aorta, and suprarenal and infrarenal abdominal aorta. An aneurysm was defined as an arterial diameter > 1.96 standard deviations above the predicted diameter [18] [19]. Probands from families 2-8 and 9-11 were referred for molecular and/or clinical evaluation to Antwerp (Belgium) or Osaka (Japan), respectively.

Screening of the entire coding region of *TGFB3* was performed in 470 additional probands (120 probands had whole exome sequencing), presenting both with syndromic and non-syndromic forms of TAAD. The majority of these patients had been screened previously for all known TAAD genes. Family members of mutation positive patients were ascertained and submitted to clinical investigations.

Genotyping and linkage analysis

Genomic DNA was extracted from peripheral blood samples (Gentra Systems). RNA from two patients (1-II:12 and III:11, **Figure 1**) was extracted from peripheral blood (collected in PAXgene tubes) according to the manufacturer's protocol (PreAnalyliX, Qiagen).

Genome-wide genotyping was conducted using DNA from 6 family members (**Figure 1**, family 1) with the Illumina Human SNP-Cyto12 Arrays, containing >262,000 genomic markers, as recommended by the manufacturer. The statistical package easyLINKAGE Plus v5.08 [20], Merlin v1.0.1 software was used to perform single point and multipoint parametric linkage analysis as previously described [21, 22]. LOD scores were obtained using a dominant model of inheritance, with penetrance of 90% and disease allele frequency of 1:1,000. Allele frequencies of genotyped SNPs were set to co-dominant and spacing of 0.25 Mb to 0.15 Mb between SNPs was used. Haplotype blocks containing 100 SNPs were constructed with Merlin (option BEST) and they were visualized using HaploPainter.

Sequencing and mutation analysis

For 120 patients exome sequencing was performed after TruSeq Exome enrichment on HiSeq (Illumina). In 350 other probands, bidirectional Sanger sequencing of exons and exon-intron boundaries was undertaken using PCR primers designed by Primer3 software (**Supplemental Table 1**). PCR products were purified and sequenced using BigDye Terminator chemistry v3.1 on an ABI Prism3130xl (Applied Biosystems). Sequences were aligned (SeqScape v2.5 software, Applied Biosystems) and compared with consensus sequences obtained from the human genome databases (Ensembl and NCBI). For annotation of DNA and protein changes, the Mutation Nomenclature guidelines from the Human Genome Variation Society (HGVS) were followed. To describe mutations at the cDNA level, the A from the ATG start codon of the reference sequences is numbered as 1 (mRNA NM_003239.2 and protein NP_003230.1).

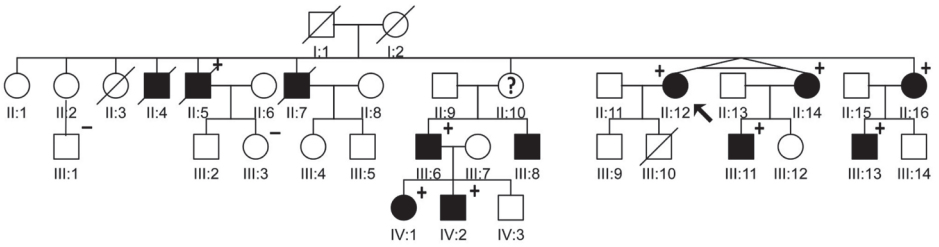

Fam 1: c.754+2T>C; p.Glu216_Lys251del

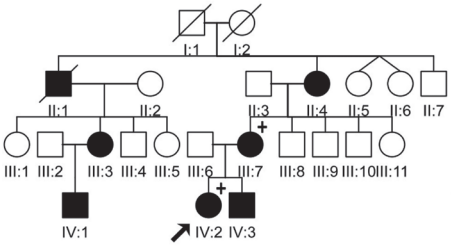

Fam 2: c.898C>T; p.Arg300Trp

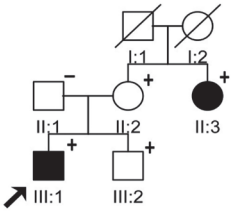

Fam 3: c.787G>C; p.Asp263His

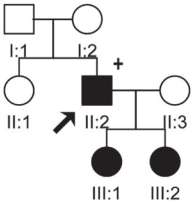

Fam 4: c.898C>T; p.Arg300Trp

Fig 1 (cont).

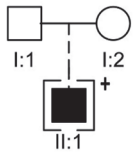

Fam 5: c.898C>T; p.Arg300Trp

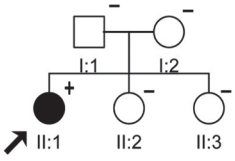

Fam 6: c.1095C>A; p.Tyr365*

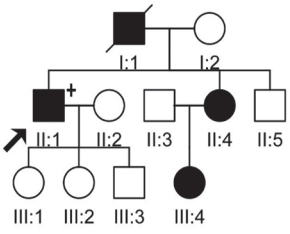

Fam 7: c.1157delT; p.Leu386Argfs*21

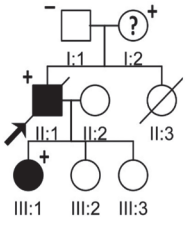

Fam 8: c.1202T>C; p.Leu401Pro

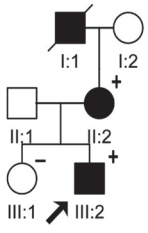

Fam 9: c.704delA; p.Asn235Metfs*11

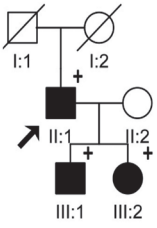

Fam 10: c.965T>C; p.Ile322Thr

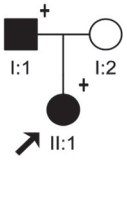

Fam 11: c.898C>T; p.Arg300Trp

Figure 1. Overview of the families with *TGFB3* mutations. The causal *TGFB3* mutation is shown for each family. The probands are indicated with an arrow. The genotype is indicated at the top right corner of the symbol. Circle: female; square: male; open symbol: unaffected; filled symbol: affected; diagonal line: deceased; brackets: adopted; question mark: clinical affection status unknown. The plus and minus signs indicate presence or absence of a *TGFB3* mutation, respectively.

In silico analysis of novel variants

The effects of the mutations on the protein structure and function were predicted using SIFT Blink and Mutation Taster. Population frequencies in controls were obtained from dbSNP, Exome Variant Server (EVS), 1000Genomes, and Genome of the Netherlands. To assess the putative effects on splicing, the Splice Site Prediction by Neural Network [23], the NetGene2 [24] and Alamut Software Suite were used. Protein ID's used for conservation were gi|148342461 (ABQ59024.1), gi|135685 (P17125.1), gi|18266825 (P16047.2), gi|135682 (P17247.1), gi|52138563 (NP_919367.2), gi|410898023 (XP_003962498.1), gi|351050916 (CCD74236.1), gi|17137520 (NP_477340.1), gi|135674 (P01137.2) and gi|48429157 (P61812.1).

Homology modelling

A homology model was built using the experimentally solved structure of TGFB1 (PDB file [25] 3rjr, 60% identity) as a template. The model was built using an automatic YASARA script [26] with standard parameters. The model contains a homo-dimer of residues 14-412.

Immunohistochemistry

The protocol for staining of formalin-fixed, paraffin-embedded sections was adapted from Baschong *et al* [27] with modifications (Detailed Methods, **Supplemental Information**). Slides were stained overnight at 40°C with anti-pSmad2 antibody (clone A5S, Millipore, Cat. # 04-953, 1:100) and anti-pERK1/2 (clone D13.14.4E, Cell Signaling, Cat. # 4370, 1:100) in 0.1% Triton/TBS buffer, washed 3x10min in Perm/Staining buffer, and then stained with anti-rabbit Alexa594 (Molecular Probes) at 1:200 for 1h at RT. Slides were then washed 3x10min in Perm/Staining buffer and mounted with Hard Set VECTASHIELD® Mounting Media with DAPI. Images were acquired on a Zeiss AxioExaminer with 710NLO-Meta multiphoton confocal microscope at 25x magnification.

In situ RNA with ACD® RNAscope probes

The ACD® RNAscope probe Hs-TGFB1 probe (cat#400881) was used to detect human *TGFB1* transcript in conjunction with the RNAscope® 2.0 HD Reagent Kit (RED) from ACD® (Detailed Methods, **Supplemental Information**).

Histology

Slides were histologically examined after Hematoxylin-Eosin, elastica von Gieson (elastin), Alcian blue (proteoglycans), Masson's trichrome (collagen) staining using standard techniques.

Results

We studied a large Dutch family (family 1) with clinical features overlapping with MFS and LDS consistent with an autosomal dominant inheritance pattern. Seven family members, between 40 and 68 years of age, presented with aneurysms and dissections, mainly involving the descending thoracic and abdominal aorta (**Figure 1** and **Supplemental Table 2**). Three patients died from aortic dissection and rupture of the descending thoracic or abdominal aorta (1-II:4, II:5, and II:7, **Figure 1**), which was confirmed by autopsy in two cases (1-II:4, 57 years and II:5, 56 years). In addition, four members had mitral valve abnormalities, ranging from mild mitral valve prolapse to severe regurgitation requiring surgical intervention. Craniofacial abnormalities were rather subtle, including a long face, high-arched palate and retrognathia (**Figure 2**). Pectus deformity and scoliosis were frequently observed. Other recurrent findings included velvety skin, varices and hiatal hernia. Several family members presented with autoimmune features including (HLA-B27 positive) spondyloarthritis, Graves' disease and celiac disease.
Sequencing of all known TAAD genes (*ACTA2, COL3A1, EFEMP2, FBN1*, *FLNA, MYH11*, *MYLK, NOTCH1*, *PRKG1, SKI, SLC2A10*, *SMAD3*, *TGFB2*, *TGFBR1*, *TGFBR2*) failed to identify a causal muta-

Figure 2. Phenotypic characteristics of patients with a *TGFB3* mutation. The clinical features observed include long face (1-III:11, 5-II:1, 7-II:1, 8-II:1), pectus carinatum (1-IV:2), hypertelorism (2-III:7, 2-IV:2, 2-IV:3, 7-II:1, 8-II:1), bifid uvula (2-III:7, 2-IV:3, 7-II:1), joint hypermobility (2-IV:2), arachnodactyly (5-II:1) and metatarsus adductus (8-III:1).

tion. Linkage analysis using SNP genotypes from six patients of the family identified two large genomic regions on chromosomes 14 and 15 shared by all affected patients (**Supplemental Figure 1**). Detailed inspection of the genes in the regions identified several candidates, most prominently the *TGFB3* gene on 14q24. Subsequent Sanger sequencing of all 7 exons and intron boundaries identified a heterozygous intronic variant affecting the highly conserved (PhastCons: 1, PhyloP: 4.97) canonical donor splice site of exon 4 (c.754+2T>C), which is absent from variant databases (Exome Variant Server, Genome of the Netherlands, 1000Genomes). cDNA sequencing for two patients (1-II:12 and III:11) confirmed skipping of exon 4, leading to an in-frame deletion of 108 nucleotides (**Supplemental Figure 2**). At the protein level, a deletion of 36 amino acids is expected (p.Glu216_Lys251del). This *TGFB3* mutation (c.754+2T>C) segregated with the clinical phenotype and was also present in one young individual (1-IV:1, 17 years old) without documented cardiovascular features (**Figure 1** and **Supplemental Table 2**) but mild systemic manifestations including craniofacial features, easy bruising and scoliosis.

To further investigate the role of *TGFB3* in TAAD etiology, DNA samples from 350 syndromic and non-syndromic TAAD probands were Sanger sequenced for mutations in all exon-intron boundaries and the coding region of *TGFB3.* Additionally, in 120 TAAD patients a targeted analysis of TAAD candidate genes after whole exome sequencing was performed. This revealed additional heterozygous *TGFB3* mutations in 10 other probands (seven from Sanger-sequencing and three from the exome sequencing cohort): four different missense mutations, p.Asp263His (family 3), p.Arg300Trp (families 2,4,5,11), p.Ile322Thr (family 10), p.Leu401Pro (family 8); one nonsense mutation, p.Tyr365* (family 6) and two single base deletions leading to a frameshift and premature stopcodon, p.Leu386Argfs*21 (family 7) and p.Asn235Metfs*11 (family 9) (**Figure 3**). All missense mutations were predicted as deleterious by SIFT [28] and as disease causing by Mutation Taster [29]. The two missense mutations in exon 5 (p.Asp263His and p.Arg300Trp) are both affecting highly conserved amino acids of the latency associated peptide (LAP) domain, which are also conserved among the TGFB1, TGFB2 and TGFB3 proteins (**Figure 3**). The p.Asp263His alteration disrupts the Arg-Gly-Asp (RGD) motif which is essential for binding to the αvß3, αvß6, αvß1 and αvß5 integrins [30-32]. Mutations of the RGD motif in LAPβ3 were demonstrated to abolish binding to αvß3, αvß5 and αvß6 [32]. The second missense mutation in exon 5, p.Arg300Trp, affects the last amino acid of the LAP domain, thus disrupting the last residue of the RKKR minimal recognition motif of the furin or related protease cleavage site [33]. Mutations affecting similar amino acids in TGFB2 have been shown to be causal in syndromic forms of aortic aneurysms [8]. The two other missense mutations, p.Ile322Thr and p.Leu401Pro, are affecting highly conserved amino acids located in the region of the active cytokine itself. The three other mutations create premature stop codons either in the LAP or the active TGFB3 (cytokine) domain, leading to nonsense mediated decay or truncated proteins which probably lose their cytokine activity.

The causal nature of the *TGFB3* mutations was further supported by *de novo* occurrence (family 6, **Figure 1**) and absence from controls (all mutations) in EVS, 1000 Genomes and the Genome of the Netherlands (GoNL). Although p.Tyr365* in family 6 occurred *de novo*, we previously identified a *SMAD3* variant (p.Ala250Thr) of unknown significance in the proband. This *SMAD3* variant was also present in the proband's mother who presented with variable connective tissue findings and mild cardiovascular involvement making its precise contribution to pathogenesis unclear.

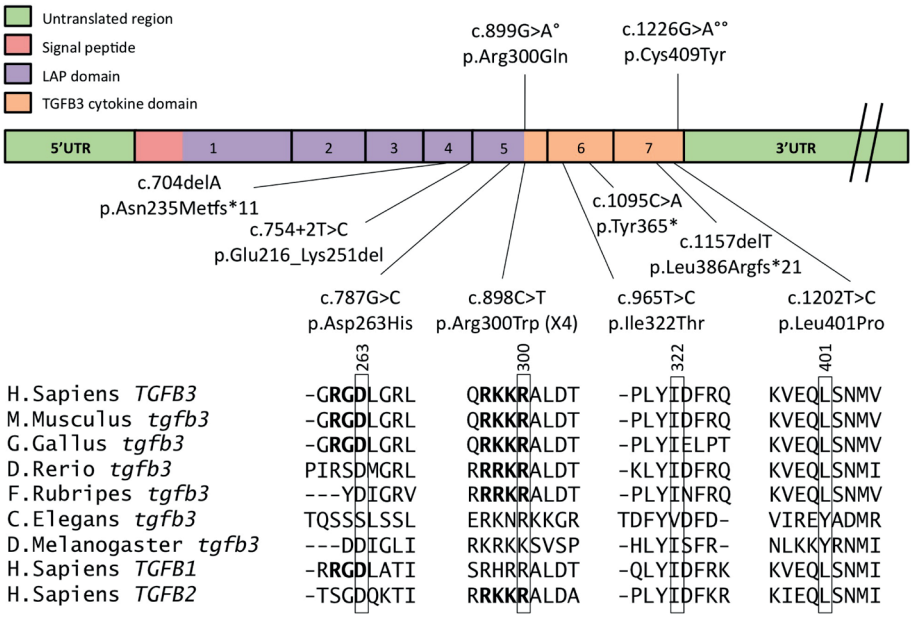

Figure 3. Mutation overview of the *TGFB3* gene. Exons are represented by rectangles. The exon numbering is given and different colors denote the different protein domains. Mutations found in this study are indicated below the gene in the respective domains. Evolutionary conservation in TGFB3 and its related proteins is given for the four missense mutations (p.Arg300Trp: Family 2, 4, 5 and 11; p.Asp263His: Family 3; p.Leu401Pro: Family 8; p.Ile322Thr: Family 10). The previously published mutations are shown above the gene and are indicated with ° from Matyas et al. (17) and °° from Rienhoff et al. (16).

We studied the molecular effects of these mutations in more detail using a homology model of the TGFB3 dimer. Asp263 is located in a surface loop where it is accessible for integrins (**Figure 4**). Mutation p.Glu216_Lys251del results in deletion of a central beta-strand and subsequent surface loop in the LAP domain (**Figure 4**). This will severely affect the conformation of this domain, including the position of the RGD motif, and thereby affect dimerization and inhibition of the TGFB3 domain. Missense mutations p.Arg300Trp, p.Ile322Thr and p.Leu401Pro are also predicted to alter TGFB3 function. Besides participating in the cleavage site, the Arg300 is involved in several ionic interactions that will be lost with the substitution to Tryptophan and this bulky residue will likely induce sterical rearrangements. The Ile322Thr

is predicted to alter the positioning of Arg325, an important amino acid residue for binding with TGFBR2. In addition, hydrophobic contacts with the N-terminal helix in the LAP domain will be affected by the substitution by Threonine (hydrophilic). Substitution from Leu401 to Proline is predicted to change the hydrophobic interactions with residues of both the LAP and TGFB3 domain.

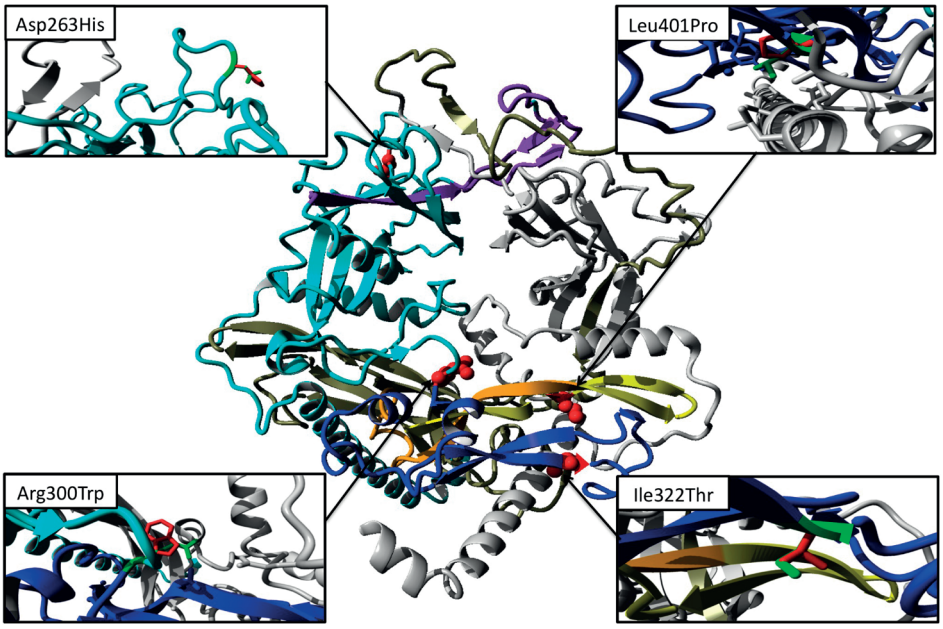

Figure 4. Overview of the TGFB3 dimer model and mutations. One monomer is shown in grey. The other monomer is shown in cyan (LAP domain) and blue (TGFB3 domain). Residues deleted by the p.Glu216_Lys251del mutation are shown in purple. Residues affected by the p.Leu386Argfs21* mutation are shown in yellow (note that this mutation also adds 21 different residues which cannot be modeled). Residues deleted by the p.Tyr365* mutation are shown in orange and yellow (note that this mutation deletes all residues that follow Tyr365). Residues deleted by mutation p.Asn235Metfs*11 is shown as grey-olive in the second monomer (note that this mutation also adds 11 different new residues which cannot be modelled). The point mutations p.Asp263His, p.Arg300Trp, p.Ile322Thr, and p.Leu401Pro are shown in red with their side-chains visible as red balls. A detailed close-up of these mutations is shown in four extra panels. In these panels the wild-type residue side chain is shown in green whereas the mutant side-chain is shown in red. For the p.Arg300Trp mutation, side chains of nearby negative residues are shown as well. For the p.Leu401Pro mutation, nearby hydrophobic residues are shown.

The clinical phenotype in the 10 additional families demonstrates a significant overlap with Loeys-Dietz syndrome (**Supplemental Tables 3-6**). Vascular involvement ranges from no cardiovascular abnormalities at age 64 (3-II:2) to type A (median age of 51 years, range 40-80) or type B aortic dissection (median age of 44.5 years, range 30-57), abdominal aortic dissection and death due to cerebral aneurysm dissection at age 55 (2-II:1) (**Table 1**). So far, no examples of early arterial dissection or dissection at small aortic dimension were observed. Other cardiovascular features include mitral valve disease, ranging from mild insufficiency to chorda rupture necessitating surgery and persistent foramen ovale, atrial or ventricular septal

defects (ASD or VSD). Disease beyond the aorta with iliac and subclavian artery aneurysms was only identified in two patients (1-II:12 and 1-III:13). No striking aortic or arterial tortuosity was observed. Typical LDS findings such as hypertelorism, bifid uvula and cleft palate, cervical spine instability and club foot deformity are commonly observed (**Figure 2**, **Table 1**, **Table 2** and **Supplemental Tables 3-6**). Other recurrent features include dolichocephaly, high-arched palate, retrognathia (with surgery in case 3-III:1), tall stature, joint hypermobility, arachnodactyly, pectus deformity and inguinal hernia (**Table 1** and **Figure 2**). No evidence for ectopia lentis was found in the medical records. Early-onset osteoarthritis was only reported in two individuals (10-II:1 and 11-II:1). The clinical features from 43 identified patients belonging to 11 families are summarized in **Table 1**. We observed a striking intra- and interfamilial clinical variability with typical LDS features in some but complete absence in others.

Table 1. Patient characteristics

Clinical features	**Affected individuals (n=43)** *
Sex (M/F)	23 M / 20 F
Median age (range)	34 years (3-74)
Median age at death (range)	56 years (40-80)
Median age at dissection (range)	47.5 years (30-80)
Cardiovascular findings	
Type A dissections (median; age range)	n=4 (51; 40-80 years)
Type B dissections (median; age range)	n=6 (44.5; 30-57 years)
Aortic aneurysm (median; age range)	n=6 (34; 3-68 years)
Abdominal aortic surgery	n=2 (43 and 50 years)
Disease beyond aorta	n=3 (cerebral, iliac, subclavian)
Skeletal findings	
Tall stature	n=12
Arachnodactyly	n=16
Pectus deformity	n=8
Kyphoscoliosis	n=11
Joint hypermobility	n=9
Loeys-Dietz features	
Hypertelorism	n=14
Bifid uvula	n=11
Cleft palate	n=5

*Not all patients have been evaluated for all features.

We subsequently investigated the effect of the p.Asp263His mutation on aortic wall architecture and TGFβ signaling. Microscopic examination of the dissected aortic wall, obtained at the time of surgery (3-III:1), showed elastic fiber fragmentation with higher collagen and proteoglycan deposition (**Figures 5A-5C**). These histopathological findings are highly reminiscent of both MFS and LDS [8]. Retrieved pathology reports from two patients (1-II:4 and II:5) carrying the p.Glu216_Lys251del mutation (family 1) also described extensive elastic fiber

fragmentation with "pseudo cyst formation" in the medial layer of the dissected aorta and "aortic medial degeneration". In families 9 and 10, only mild elastic fiber fragmentation was observed. To investigate TGFβ signaling in the aortic wall of a patient carrying a *TGFB3* mutation (p.Asp263His), we performed immunohistochemical analysis of aortic tissue (**Figures 5D-5F**). Very similar to what has been detected in TGFB2 deficient aortic walls of humans and mice [8], we observed evidence for paradoxically enhanced TGFβ signaling in the aortic wall of a *TGFB3* mutant patient, as shown by increased pSMAD2 (canonical TGFβ signaling), pERK (non-canonical TGFβ signaling) and elevated *TGFB1* RNA messenger (**Figures 5D-5F**).

Table 2. Phenotypical characteristics of patients with *TGFBR1/2, SMAD3, TGFB2 and TGFB3* mutations

Phenotype	***TGFBR1 TGFBR2***	***SMAD3***	***TGFB2***	***TGFB3***
Hypertelorism	+	+	+	+
Bifid uvula/cleft palate	+	+	+	+
Exotropia	+	+	+	+
Craniosynostosis	+	+	–	–
Cervical spine instability	+	+	–	+
Retrognathia surgery	+	+	+	+
Scoliosis/spondylolisthesis	+	+	+	+
Clubfoot	+	+	+	+
Osteoarthritis	+	+	–	+
Dural ectasia	+	+	+	?
Pneumothorax	+	+	+	–
Hernia	+	+	+	+
Dissection at young age	+	+	+	?
Disease beyond root	+	+	+	+
Cerebral hemorrhage	+	+	+	+
Arterial tortuosity	+	+	+	–
Autoimmune findings	+	+	+	+

+ indicates presence of the clinical feature, – indicates absence of the clinical feature, and ? indicates presence of a clinical feature is unknown.

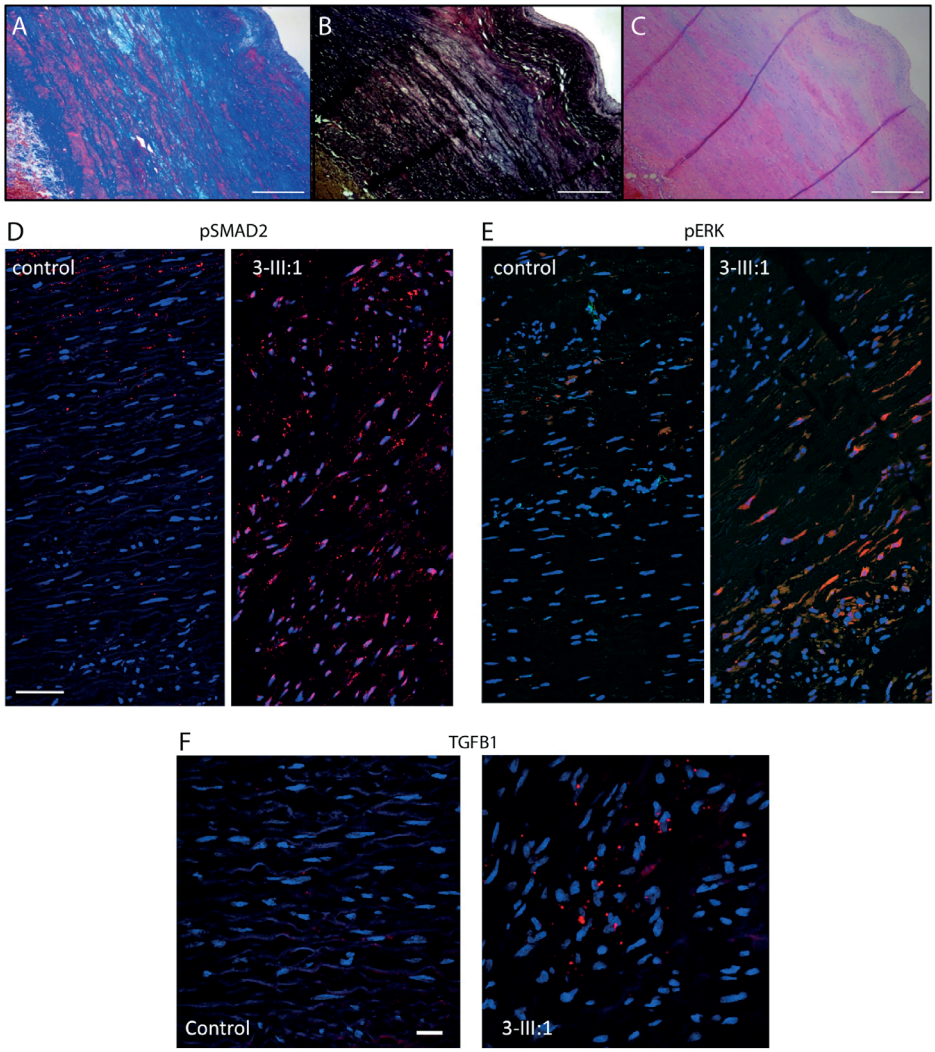

Figure 5. Cardiovascular pathology and immunohistochemical analysis of TGFB family proteins in a human subject with *TGFB3* mutation (3-III:1; p.Asp263His). (A) Masson trichrome staining shows increased deposition of collagen (dark blue) and loss of smooth muscle fibers (red) in the media. (B) Elastin stain (elastica von Gieson) shows loss of elastin fibers (black). (C) Hematoxylin-eosin staining shows deposition of proteoglycan (light blue) in the media. (A-C) scale bar 2mm. (D-F) Cross-sections of the media of the aortic wall of patient 3-III:1 and a matched control. Red staining corresponds to (D) pSmad2, (E) pERK and (F) TGFB1. (D-E) scale bar 50 µm, (F) scale bar 20 µm. Blue staining shows cell nuclei (DAPI), co-localization is purple. Red staining not co-localized with DAPI is non-specific.

Discussion

During mouse embryonic development, *Tgfb3* is expressed in several tissues, including cardiovascular, pulmonary, skin and craniofacial structures. Although *Tgfb3* is expressed in overlapping fashion with *Tgfb2* in the cardiovascular system, most attention has been paid

to its role in palatogenesis as *Tgfb3* knockout mice die at birth due to cleft palate [34, 35]. No major cardiac developmental defects have been reported in *Tgfb3* deficient mice [34, 36, 37]. Although minor abnormalities at the aortic arch level, as well as in position and curvature of the aortic arches and myocardial architecture have been described in the *Tgfb3* knockout mice, no data are available on the aortic sizes of conditional knockout or haplo-insufficient animals [35, 36]. Of interest, the presence of aortic aneurysms and ruptures recapitulating the human phenotype were previously overlooked upon the initial phenotypic description of *Tgfb2* haplo-insufficient and *Smad3* knockout mouse models [8, 26].

Because we observed three truncating mutations and an in frame splice site mutation, we hypothesize that the *TGFB3* mutations lead to loss of function (LOF) of TGFB3. In addition, two missense mutations, located in the LAP domain, alter critical residues that are relevant for TGFB3 activation by integrins and TGFB3 processing [31, 38]. Mice carrying a missense mutation affecting the RGD integrin-binding motif of Tgfb1 recapitulate the phenotype of Tgfb1 knockout mice [39], suggesting that the *TGFB3* mutation disrupting the RGD (p.Arg263His) might also lead to LOF. Similarly, molecular analyses and predictions based on the TGFB3 dimer model confirm that most of the *TGFB3* mutations reported here are causing LOF. Although it was previously hypothesized that patients with LOF mutations in *TGFB3* lack cardiovascular phenotypes [16], we here clearly demonstrate that *TGFB3* LOF mutations associate with aortic and other arterial aneurysms/dissections and mitral valve disease. We recognize an extremely variable cardiovascular phenotype in the *TGFB3* cohort described here. The relatively young age of the previously reported patients with *TGFB3* mutations (8 years old [16] and 10.5 years old [17]) might explain the lack of obvious cardiovascular disease. Rienhoff et al. hypothesized that the mutated, inactivated allele (p.Cys409Tyr) leads to a non-functional protein, which causes a decrease of both canonical and non-canonical TGFβ signaling based on expression studies of the mutant TGFB3 protein in a Xenopus model. In contrast, our experiments on human aortic tissue reveal a signature of increased TGFβ signaling. These findings confirm our prior experience that mutational hits in the TGFBR1/2 receptors, the SMAD3 signal transducer or the TGFB2 ligand lead to a paradoxical increase in TGFβ signaling as evidenced here by increased immunohistochemical signals for pSMAD2, pERK and TGFB1 [5, 7, 8]. The exact nature of this paradoxical effect needs further study but shifts in balances between canonical (pSMAD2) and non-canonical (pERK) cascades, classic and alternative (BMP driven) TGFβ superfamily cascades as well as shifts in ligand expression (TGFB1 versus TGFB2 or TGFB3) seem likely to be important contributing factors [40, 41].

TGFB3 mutations also appear to have opposing effects on height as one patient in this study (3-III:1, p.Asp263His) has short stature and received growth hormone therapy during puberty and the patient reported by Rienhoff et al. (pCys409Tyr) presented with short stature (5th centile), whereas others (several patients in this study and the patient reported by Matyas et

al. [17]) presented with tall stature. *TGFB3* mutations affecting residue Arg300 are associated with cleft palate and/or bifid uvula in our patients (**Supplemental Tables 3, 4 and 6**) and in the patient reported by Matyas et al [17]. Our study confirms the association of *TGFB3* mutation with overt cleft palate in humans and as such endorses its important role in palatogenesis.

Although our experience is limited to 43 patients in 11 families, our findings warrant a comprehensive cardiovascular imaging of the patients. So far, no strong evidence has emerged for early aortic dissection in *TGFB3* mutant patients but as the phenotypical spectrum associated with *TGFBR1/2, SMAD3* and *TGFB2* has now also been demonstrated to be extremely wide, we cannot rule out the occurrence of early catastrophic events. We would recommend yearly echocardiographical evaluation of the aortic root in all mutation carriers complemented with at least one baseline imaging of the complete aorta and side branches. Frequency of follow-up should be guided by initial findings, family history and experience still to be gained. Depending of family history and future knowledge, additional imaging of the brain vessels might be indicated. Furthermore, the true incidence and full spectrum of autoimmune manifestations in *TGFB3* mutation carriers should be determined in follow-up studies.

Conclusions

We demonstrate that mutations in the *TGFB3* ligand are responsible for a syndromic form of aortic aneurysmal disease. Our study also provides evidence for a paradoxical increase in TGFβ signaling in the aorta, in keeping with our previous findings in *TGFBR1/2*, *SMAD3* and *TGFB2* mutation carriers. The clinical histories of the patients in our cohort warrant lifelong and widespread cardiovascular surveillance in patients with *TGFB3* mutations. Further research explaining the wide clinical variability is strongly indicated.

Acknowledgments

The authors are grateful to the families and patients that participated in this study. We acknowledge Christoph Hermans (Department of Pathology, Antwerp University Hospital) for technical support, Josephina Meester (Center for Medical Genetics, University of Antwerp) and Tom Vries Lentsch (Erasmus University Medical Center) for helping with the art work, Akiko Yoshida and Razia Sultana (Departments of Bioscience and Genetics, National Cerebral and Cardiovascular Center, Suita, Osaka, Japan) for genetic analysis and Tatsuya Oda, Hiroshi Tanaka and Hiroaki Sasaki (Department of Cardiovascular Surgery, National Cerebral and Cardiovascular Center, Suita, Osaka, Japan) for patient management.

References

1. Massague J. TGFbeta signalling in context. Nat Rev Mol Cell Biol 2012;13:616-30.
2. Neptune ER, Frischmeyer PA, Arking DE et al. Dysregulation of TGF-beta activation contributes to pathogenesis in Marfan syndrome. Nat Genet 2003;33:407-11.
3. Habashi JP, Judge DP, Holm TM et al. Losartan, an AT1 antagonist, prevents aortic aneurysm in a mouse model of Marfan syndrome. Science 2006;312:117-21.
4. Dietz HC, Cutting GR, Pyeritz RE et al. Marfan syndrome caused by a recurrent de novo missense mutation in the fibrillin gene. Nature 1991;352:337-9.
5. Loeys BL, Chen J, Neptune ER et al. A syndrome of altered cardiovascular, craniofacial, neurocognitive and skeletal development caused by mutations in TGFBR1 or TGFBR2. Nat Genet 2005;37:275-81.
6. Mizuguchi T, Collod-Beroud G, Akiyama T et al. Heterozygous TGFBR2 mutations in Marfan syndrome. Nat Genet 2004;36:855-60.
7. van de Laar IM, Oldenburg RA, Pals G et al. Mutations in SMAD3 cause a syndromic form of aortic aneurysms and dissections with early-onset osteoarthritis. Nat Genet 2011;43:121-6. .
8. Lindsay ME, Schepers D, Bolar NA et al. Loss-of-function mutations in TGFB2 cause a syndromic presentation of thoracic aortic aneurysm. Nat Genet 2012;44:922-7.
9. Boileau C, Guo DC, Hanna N et al. TGFB2 mutations cause familial thoracic aortic aneurysms and dissections associated with mild systemic features of Marfan syndrome. Nat Genet 2012;44:916-921.
10. Doyle AJ, Doyle JJ, Bessling SL et al. Mutations in the TGF-beta repressor SKI cause Shprintzen-Goldberg syndrome with aortic aneurysm. Nat Genet 2012;44:1249-54.
11. Loeys BL, Schwarze U, Holm T et al. Aneurysm syndromes caused by mutations in the TGF-beta receptor. N Engl J Med 2006;355:788-98.
12. van de Laar IM, van der Linde D, Oei EH et al. Phenotypic spectrum of the SMAD3-related aneurysms-osteoarthritis syndrome. J Med Genet 2012;49:47-57.
13. van der Linde D, van de Laar IM, Bertoli-Avella AM et al. Aggressive cardiovascular phenotype of aneurysms-osteoarthritis syndrome caused by pathogenic SMAD3 variants. J Am Coll Cardiol 2012;60: 397-403.
14. Shprintzen RJ, Goldberg RB. A recurrent pattern syndrome of craniosynostosis associated with arachnodactyly and abdominal hernias. J Craniofac Genet Dev Biol 1982;2:65-74.
15. Rienhoff HY, Jr. Response to "De novo mutation of the TGFB3 latency-associated peptide domain in a patient with overgrowth and Loeys-Dietz syndrome features". Am J Med Genet A 2014.
16. Rienhoff HY, Jr., Yeo CY, Morissette R et al. A mutation in TGFB3 associated with a syndrome of low muscle mass, growth retardation, distal arthrogryposis and clinical features overlapping with Marfan and Loeys-Dietz syndrome. Am J Med Genet A 2013;161A:2040-6.
17. Matyas G, Naef P, Tollens M, Oexle K. De novo mutation of the latency-associated peptide domain of TGFB3 in a patient with overgrowth and Loeys-Dietz syndrome features. Am J Med Genet A 2014.
18. Campens L, Demulier L, De Groote K et al. Reference values for echocardiographic assessment of the diameter of the aortic root and ascending aorta spanning all age categories. Am J Cardiol 2014;114: 914-20.
19. Rogers IS, Massaro JM, Truong QA et al. Distribution, determinants, and normal reference values of thoracic and abdominal aortic diameters by computed tomography (from the Framingham Heart Study). Am J Cardiol 2013;111:1510-6.
20. Hoffmann K, Lindner TH. easyLINKAGE-Plus--automated linkage analyses using large-scale SNP data. Bioinformatics 2005;21:3565-7.
21. van de Laar I, Wessels M, Frohn-Mulder I et al. First locus for primary pulmonary vein stenosis maps to chromosome 2q. Eur Heart J 2009;30:2485-92. .
22. Thiele H, Nurnberg P. HaploPainter: a tool for drawing pedigrees with complex haplotypes. Bioinformatics 2005;21:1730-2.

23. Reese MG, Eeckman FH, Kulp D, Haussler D. Improved splice site detection in Genie. J Comput Biol 1997; 4:311-23.
24. Brunak S, Engelbrecht J, Knudsen S. Prediction of human mRNA donor and acceptor sites from the DNA sequence. J Mol Biol 1991;220:49-65.
25. Shi M, Zhu J, Wang R et al. Latent TGF-beta structure and activation. Nature 2011;474:343-9.
26. Krieger E, Vriend G. YASARA View-molecular graphics for all devices-from smartphones to workstations. Bioinformatics 2014.
27. Baschong W, Suetterlin R, Laeng RH. Control of autofluorescence of archival formaldehyde-fixed, paraffin-embedded tissue in confocal laser scanning microscopy (CLSM). J Histochem Cytochem 2001;49:1565-72.
28. Ng PC, Henikoff S. Predicting deleterious amino acid substitutions. Genome Res 2001;11:863-74.
29. Schwarz JM, Cooper DN, Schuelke M, Seelow D. MutationTaster2: mutation prediction for the deep-sequencing age. Nat Methods 2014;11:361-2.
30. Munger JS, Harpel JG, Giancotti FG, Rifkin DB. Interactions between growth factors and integrins: latent forms of transforming growth factor-beta are ligands for the integrin alphavbeta1. Mol Biol Cell 1998;9: 2627-38.
31. Annes JP, Rifkin DB, Munger JS. The integrin alphaVbeta6 binds and activates latent TGFbeta3. FEBS Lett 2002;511:65-8.
32. Ludbrook SB, Barry ST, Delves CJ, Horgan CM. The integrin alphavbeta3 is a receptor for the latency-associated peptides of transforming growth factors beta1 and beta3. Biochem J 2003;369:311-8.
33. Constam DB. Regulation of TGFbeta and related signals by precursor processing. Semin Cell Dev Biol 2014;32C:85-97.
34. Kaartinen V, Voncken JW, Shuler C et al. Abnormal lung development and cleft palate in mice lacking TGF-beta 3 indicates defects of epithelial-mesenchymal interaction. Nat Genet 1995;11:415-21.
35. Azhar M, Schultz Jel J, Grupp I et al. Transforming growth factor beta in cardiovascular development and function. Cytokine Growth Factor Rev 2003;14:391-407.
36. Doetschman T, Georgieva T, Li H et al. Generation of mice with a conditional allele for the transforming growth factor beta3 gene. Genesis 2012;50:59-66.
37. Azhar M, Runyan RB, Gard C et al. Ligand-specific function of transforming growth factor beta in epithelial-mesenchymal transition in heart development. Dev Dyn 2009;238:431-42.
38. Worthington JJ, Klementowicz JE, Travis MA. TGFbeta: a sleeping giant awoken by integrins. Trends Biochem Sci 2011;36:47-54.
39. Yang Z, Mu Z, Dabovic B et al. Absence of integrin-mediated TGFbeta1 activation in vivo recapitulates the phenotype of TGFbeta1-null mice. J Cell Biol 2007;176:787-93.
40. Lindsay ME, Dietz HC. Lessons on the pathogenesis of aneurysm from heritable conditions. Nature 2011; 473:308-16.
41. Gallo EM, Loch DC, Habashi JP et al. Angiotensin II-dependent TGF-beta signaling contributes to Loeys-Dietz syndrome vascular pathogenesis. J Clin Invest 2014;124:448-60.

Supplemental Information

Detailed Methods

Immunohistochemistry

Protocol for staining of FFPE sections was adapted from Baschong *et al* with the following modifications. Slides were stained overnight at 40°C with anti-pSmad2 antibody (clone A5S, Millipore, Cat. # 04-953, 1:100) and anti-pERK1/2 (clone D13.14.4E, Cell Signaling, Cat. # 4370, 1:100) in 0.1% Triton/TBS buffer, washed 3x10min in Perm/Staining buffer, and then stained with anti-rabbit Alexa594 (Molecular Probes) at 1:200 for 1h at room temperature (RT). Slides were then washed 3x10min in Perm/Staining buffer and mounted with Hard Set VECTASHIELD® Mounting Media with DAPI. Images were acquired on Zeiss AxioExaminer with 710NLO-Meta multiphoton confocal microscope at a 25x magnification.

For removal of paraffin, slides were immersed in xylene (3x5 min), followed by graded ethanol treatment (3x5' 100%, 3x5' 95%, 3x5' 80%, 3x5' 70%), rinsed in water and immersed in tris buffered saline (TBS) buffer (50 mM Tris-Cl, pH 7.6, 150 mM NaCl). Antigen retrieval was performed in a rice steamer using 1M Sodium Citrate Buffer/0.1% Tween for 30 min. Slides were then cooled to RT for 20 min, rinsed in water, and transferred to TBS buffer. In order to minimize auto-fluorescence background, slides were then treated with freshly prepared "bubbling" 10mg/ml of sodium borohydrite in TBS for 30 minutes and then rinsed 3 times in TBS. Slides were then permeabilized with Perm/Staining buffer (0.1% Triton in TBS buffer) for 20 min, followed by a 20 min treatment with Fc block Reagent (Innovex Biosciences) and a 20 min treatment with Background Buster Reagent (Innovex Biosciences).

In situ RNA with ACD® RNAscope probes

The ACD® RNAscope probe Hs-TGFB1 probe (cat#400881) was used to detect human *TGFB1* transcript in conjunction with the RNAscope® 2.0 HD Reagent Kit (RED) from ACD®. FFPE sections were stained following the manufacturer recommended protocol, except that slides were counterstained with DAPI and not with hematoxilin. Red fluorescent signal was detected on Zeiss AxioExaminer with 710NLO-Meta multiphoton confocal microscope at a 25x magnification.

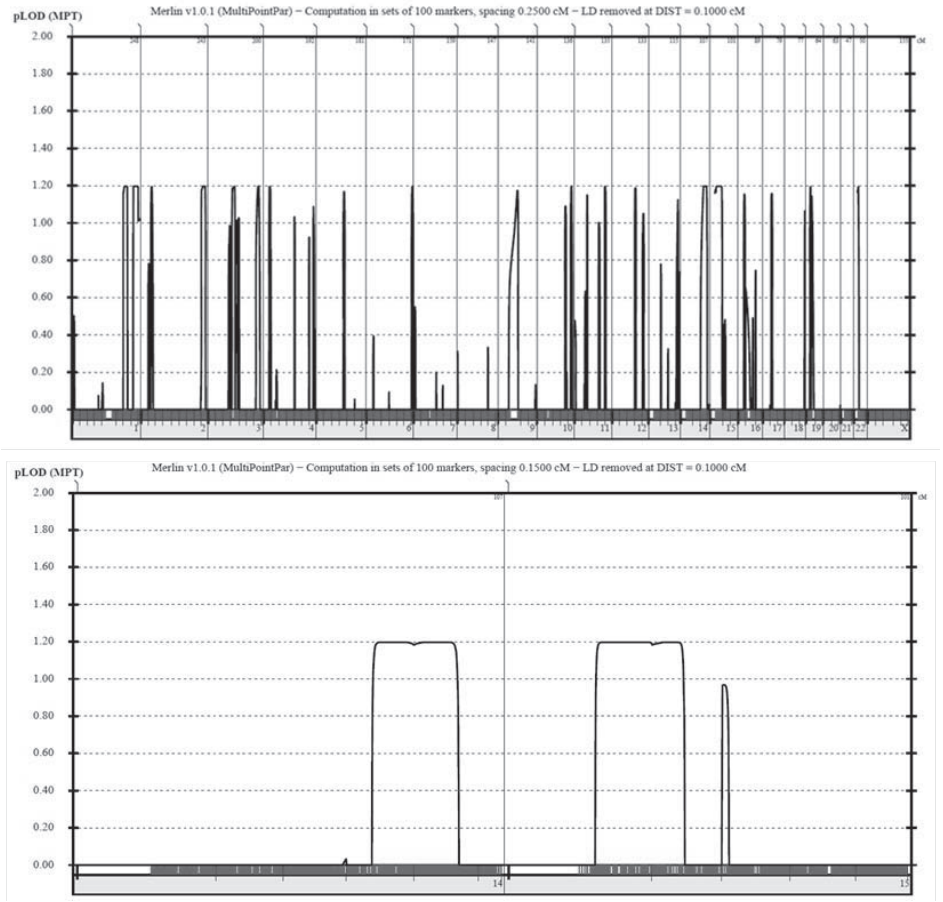

Supplemental Figure 1. Plots of the genome wide linkage analysis (upper graph) and chromosome 14 and 15 (lower graph) displaying the largest genomic regions identified. LOD scores appear in the Y-axis and chromosome numbers are on the X-axis. Vertical red lines indicate SNP coverage.

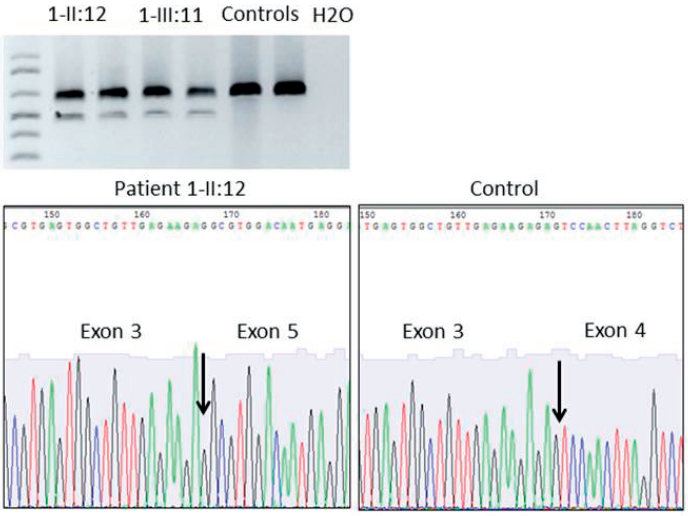

Supplemental Figure 2. To investigate the effect of the *TGFB3* c.754+2T>C variant on splicing, we designed three different PCR experiments using blood complementary DNA (cDNA) from two patients from family 1 (II:12 and III:11). The investigated fragments covered *TGFB3* exons 2-5, 3-6 and 2-6. PCR fragments corresponding to exons 2 to 5 are shown in the gel picture (in duplicate, patients in lanes 2 to 5 and normal controls in lanes 6-7). Normal expected size was 466 bp. An abnormal, smaller fragment, probably with a deletion of exon 4 was observed in the patients. Sanger sequencing using the smaller PCR band as template confirmed that the *TGFB3* c.754+2T>C mutation is leading to a deletion of exon 4 with an in-frame deletion of 108 nucleotides.

Supplemental Table 1. List of PCR primers used for Sanger sequencing

Name	Sense primer	Antisense primer	Amplicon size
TGFB3 ex1	5'-CCCTCCTTCTGCACGTCTGC-3'	5'-TCCCAGCTCCAGTTCAGACC-3'	487
TGFB3 ex2	5'-GAGGCCACACTGCTCCTTGC-3'	5'-AAACCCAGGTCTGCCAAACG-3'	469
TGFB3 ex3	5'-GAGGGCCATGGCATTCAGG-3'	5'-TGGAGGATACTCAGTGGCAAAGC-3'	391
TGFB3 ex4	5'-GCAACGTGCGCTTGAAGG-3'	5'-GGAGCTTGGTTTCTTTTCTTGAGG-3'	402
TGFB3 ex5	5'-CACGGGGCATCTTTCAGTGG-3'	5'-TGAGTGTGGCTTGGCTCTGG-3'	502
TGFB3 ex6	5'-TGGCATGAAAGGACTCCAAGG-3'	5'-TCACCCCAGACCATCATTTGC-3'	365
TGFB3 ex7	5'-GGACTGCCCCTGGAACTGG-3'	5'-TCCCTTTCCTCTATCCCCATCC-3'	532

Supplemental Table 2. Clinical characteristics of family 1 (c.754+2T>C, p.Glu216_Lys251del)

Individual	1-II:4	1-II:5*	1-II:7	1-II:10	1-III:6*	1-III:8	1-IV:1*	1-IV:2*	1-II:12*	1-II:14*	1-III:11*	1-II:16*	1-III:13*
Age	57†	56†	40†	74	51	49	17	24	72	72	47	69	44
Sex	M	M	M	F	M	M	F	M	F	F	M	F	M
Height	-	-	-	168 cm	183 cm	190 cm	181 cm	198 cm	162 cm	?	185 cm	168 cm	187 cm
Vascular	Ruptured descending TAA at age 57 AAD at age 57	Carotid artery surgery Descending TAA at age 50 Infrarenal AA at age 52	Aortic rupture at age 40	No imaging	Aortic sinus: 38 mm	Aortic sinus: 36 mm Stroke at age 48	Aortic sinus: 32 mm	No imaging	Dissection aortic arch at age 45 Aneurysm left subclavian artery at age 45	Infrarenal AA at age 68	TAA	Aortic sinus: 32 mm Ascending aorta: 35 mm	Aortic sinus: 39 mm Aneurysm right common iliac artery at age 44
Mitral valve					Mild MVP	MI with chorda rupture surgery at age 49					MVP with MI grade 3 TI grade 3		Mild MVP
Skeletal		Long face			Pectus excavatum High-arched palate Retrognathia		Mild scoliosis Mild joint laxity	Pectus carinatum surgery at age 14 High-arched palate Retrognathia	Long face		Long face Pes plani	Mild scoliosis Total hip replacement	Severe scoliosis Spondylodesis Th4-L1 Long face Retrognathia
LDS features							Soft skin Easy bruising		Thin skin Easy bruising				
Other					Varices			Varices		Hiatal hernia	Hiatal hernia	Pelvic organ prolapse Hiatal hernia Varices	

AA, aortic aneurysm; AAD, abdominal aortic dissection; TAA(D), thoracic aortic aneurysm (and dissection); MVP, mitral valve prolapse; MI, mitral insufficiency; TI, tricuspid insufficiency; Th, thoracic vertebra; L, lumbar vertebra; † deceased; * mutation present (no DNA was available from the other patients).

Supplemental Table 3. Clinical characteristics of family 2 (c.898C>T,p.Arg300Trp)

Individual	2-II:1	2-II:4	2-III:3	2-IV:1	2-III:7*	2-IV:2*	2-IV:3
Age	55†	60	26	6	31	7	6
Sex	M	F	F	M	F	F	M
Aorta	Cerebral aneurysm dissection	Normal echo	Normal echo	Aortic dilatation	Aortic sinus: 28 mm at age 29 years (Z score = -0.25)	Normal echo at age 4 years	Normal echo at age 5 years
Skeletal	Arachnodactyly Pectus excavatum	Joint hypermobility	Arm-span to height ratio > 1.05		Pectus carinatum Cervical rib	Tall stature Cervical spine instability C2-C4 Club feet Joint hypermobility Hip dysplasia	Arachnodactyly Joint hypermobility
LDS features		Bifid uvula	Bifid uvula Hypertelorism Blue sclerae	Cleft palate Hypertelorism	Bifid uvula Hypertelorism Translucent skin	Bifid uvula Hypertelorism	Bifid uvula Hypertelorism
Other						Hemiparesis – cause unknown Learning difficulties	

C, cervical vertebra; † deceased; * mutation present (no DNA was available from the other patients).

Supplemental Table 4. Clinical characteristics of families 3-6 (c.787G>C, p.Asp263His in family 3; c.898C>T,p.Arg300Trp in families 4 and 5; c.1095C>A, p.Tyr365* in family 6)

Individual	3-II:2*	3-II:3*	3-III:1*	3-III:2*	4-II:2*	4-III:1	4-III:2	5-II:1*	6-II:1*
Age	64	70	31	34	42	13	10	24	42
Sex	F	F	M	M	M	F	F	M	F
Aorta	Aortic sinus: 34 mm Mild MI	Aortic sinus: 38 mm Mild MI	TAAD at age 30 with root = 70 mm	Aortic sinus: 32 mm	Aortic sinus: 42 mm	Normal echo	Normal echo	Aortic sinus: 40 mm (Z=3.6) MVP, PFO	Normal echo
Skeletal			Dolichocephaly High-arched palate		Arachnodactyly Increased arm-span to height ratio Retrognathia Scoliosis Pes plani	Arachnodactyly Asymmetric chest Narrow palate with dental crowding		Pectus carinatum Pes plani	Arachnodactyly Joint hyperlaxity Camptodactyly toes Pes plani
LDS features			Retrognathia with surgery at age 22		Bifid uvula Hypertelorism Soft skin	Cleft palate	Cleft palate	Bifid uvula Cleft palate Hypertelorism Club foot	Bifid uvula Hypertelorism Easy bruising
Other			Delayed puberty Short stature: growth hormone therapy		Inguinal hernia surgery at age 6 years	Inguinal hernia			Delayed motor development Varices Cataract

MI, mitral insufficiency; MVP, mitral valve prolapse; PFO, patent foramen ovale; * mutation present (no DNA was available from the other patients).

Supplemental Table 5. Clinical characteristics of families 7-8 (c.1157delT, p.Leu386Argfs*21 in family 7; c.1202T>C, p.Leu401Pro in family 8)

Individual	7-I:1	7-II:1*	7-II:4	7-III:4	8-II:1*	8-III:1*
Age	70†	43	?	14	50†	30
Sex	M	M	F	F	M	F
Aorta	TAA at age 61 with TAAD at age 70	No aneurysm MVP		Normal echocardiography	Age 42: ascending aorta of 60 mm At age 43: Type A dissection with supracoronary replacement At age 44: TEVAR for type B dissection Age 50: abdominal aortic dissection	Normal echocardiography
Skeletal	Tall stature	Dolichocephaly Tall stature Arachnodactyly Scoliosis Pes plani	Tall sature Arachnodactyly	Tall stature High arched palate Arachnodactyly Scoliosis	Enlarged arm-span Arachnodacytly Dolichocephaly Mild scoliosis	Enlarged armspan Arachnodactyly Scoliosis Joint hypermobility Metatarsus adductus Camptodactyly of 4^{th}/5^{th} toes
LDS features	Cleft palate and bifid uvula	Bifid uvula Hypertelorism			Hypertelorism Spondylosis C3-C4, C5-C6 and C6-C7	
Other					Bilateral inguinal hernia surgery at age 39	

TAA(D): thoracic aortic aneurysm (and dissection); MVP, mitral valve prolapse; PFO, patent foramen ovale; C, cervical vertebra; TEVAR, thoracic endovascular aortic repair; † deceased; * mutation present (no DNA was available from the other patients).

Supplemental Table 6. Clinical characteristics of families 9-10 (c.704delA, p.Asn235Metfs*11 in family 9; c.965T>C, p.Ile322Thr in family 10; c.898C>T,p.Arg300Trp in family 11)

Individual	9-I:1	9-II:2*	9-III:1*	10-II:1*	10-III:1*	10-III:2*	11-I:1*	11-II:1*
Age	80†	67	43	56	24	22	27	3
Sex	M	F	M	M	M	F	M	F
Aorta	TAAD at age 80	TAAD type A at age 59	TAAD type A at age 40	AAA with Y-graft at age 43 TAA (47 mm) with severe AR: Bentall surgery	Aortic root 32 mm	Aortic root 34mm		VSD+ASD Aortic root aneurysm: 19.5 mm (Z>2)
Skeletal		Thin and tall habitus Arachnodactyly	Tall sature Kyphoscoliosis Pectus deformity Retrognathia Flat occiput	Tall stature Arachnodactyly Kyphoscoliosis Pectus deformity Retrognathia Downslanting palp fissures	Tall stature Arachnodacytly Scoliosis	Tall stature Arachnodactyly Joint hypermobility Kyphoscoliosis Pes plani Retrognathia Downslanting palp fissures	Tall stature Arachnodactyly Joint hypermobility High arched palate Kyphosis Pes plani	Tall stature Arachnodactlyly Joint hypermobility Retrognathia Downslanting palpebral fissures
LDS features				Hypertelorism Osteoarthritis		Hypertelorism Bifid uvula	Hypertelorism Bifid uvula Spondylolisthesis	Hypertelorism Bifid uvula Osteoarthritis Translucent skin Easy bruising
Other		Inguinal hernia Myopia			Striae			

TAA(D), thoracic aortic aneurysm (and dissection); AAA, abdominal aortic aneurysm; ASD, atrial septal defect; VSD, ventricular septal defect; † deceased; * mutation present (no DNA available on other patients).